Watermelon Tourmaline: Multivariate Analysis of Laser-Induced Breakdown Spectroscopy (LIBS) and Electron Micro-probe Analyses (EMPA)

Marie Gibson[1] and Nancy J. McMillan[1]

1. Department of Geological Sciences, New Mexico State University, Las Cruces, NM, USA

Significance

- Establishing LIBS as an effective pre-screening tool for more costly and time intensive analytical techniques, such as EMPA
- Pegmatites are a critical source of metals, REE, and gemstones. Investigating the zoning patterns in tourmalines can help us better understand the petrogenic processes that influence the geochemical evolution of a pegmatite overtime.

Introduction

Watermelon tourmaline describes a variety of tourmaline with the distinctive zoning pattern of a pink core and a green rim. This project examines compositional variations in these zoning patterns, which provide a detailed record of changes in the environment of crystallization. Previous studies (Gibson and McMillan, 2019, 2020 GSA Abstracts with Prog.) using laser-induced breakdown spectroscopy (LIBS) indicated that the green zones are enriched in Mn, which is commonly purported to be a chromophore in the pink zone; however, here we see lower Mn concentrations in the pink zones. Similar results were observed by Tollefson and Ihinger (2017, 2018 GSA Abstracts with Prog.) with the possible explanation that the oxidation state of Mn, rather than concentration, plays a large role in producing color. To better understand these zoning patterns, zoned elbaite-fluorelbaite tourmalines from various localities were investigated using EMPA and LIBS.

Methods & Materials

Zoned elbaite-fluorelbaite tourmalines from the Brown Derby Mine in the United States of America (US2A), Otjua Mine in Namibia (NM1B), Malhan Mountains in Russia (RU1A), and the Himalaya Mine in the United States of America (US1A) prepared as one-inch micro-probe polished rounds

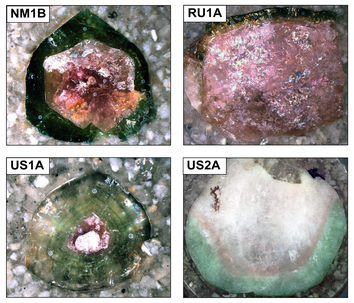

Laser-Induced Breakdown Spectroscopy (LIBS)

- *Six spectra were acquired from the core and rim zones of each sample using the Applied Spectra J200 LIBS instrument, Andor Mechelle ME5000 spectrometer, Andor IStar DH334T-18F-03 intensified CCD camera, and Q-switched 266 nm laser (Quantel ULTRA Big Sky Laser Series ULTRA 100) at Materialytics (Killeen, TX); these spectra were then normalized to total intensity for use in PCA.

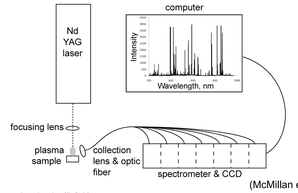

(McMillan et al., 2012)

Principal Component Analysis (PCA)

- PCA discerns relationships within a complex dataset and reduces the variability to a manageable number of variables by calculating linear regressions through the dataset, called principal components.
- A PCA score plot is a scatter plot in which data points are plotted within the space defined by two principal components (PC); spectra that cluster together are compositionally similar and those that are far apart are dissimilar.
- PCA loading plots show the relative influence of each variable (i.e., wavelength) on the direction of the PC through the dataset.
- Loading plots were data-mined to determine whether evidence for chemical exchange vectors was present in the LIBS dataset.

Electron Micro-probe Analysis (EMPA)

- *Three sites per zone were quantitatively analyzed by wavelength-dispersive spectrometry (WDS) using the automated JEOL 733 electron micro-probe at Louisiana State University. All tourmaline analyses were performed using an accelerating voltage of 15 kV and a beam current of 20 nA.
- EMPA was used to identify the wt% oxide of major and trace elements: Si, Al, Ti, V, Cr, Fe, Mn, Mg, Zn, Cu, Ca, Ba, Na, K, and F.
- Normalization and stoichiometry were used to convert wt% oxide values to atomic proportions (Henry and Dutrow, 1996).

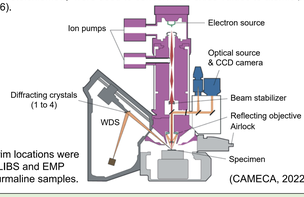

*Similar core and rim locations were selected for both LIBS and EMP analysis of the tourmaline samples.

(CAMECA, 2022)

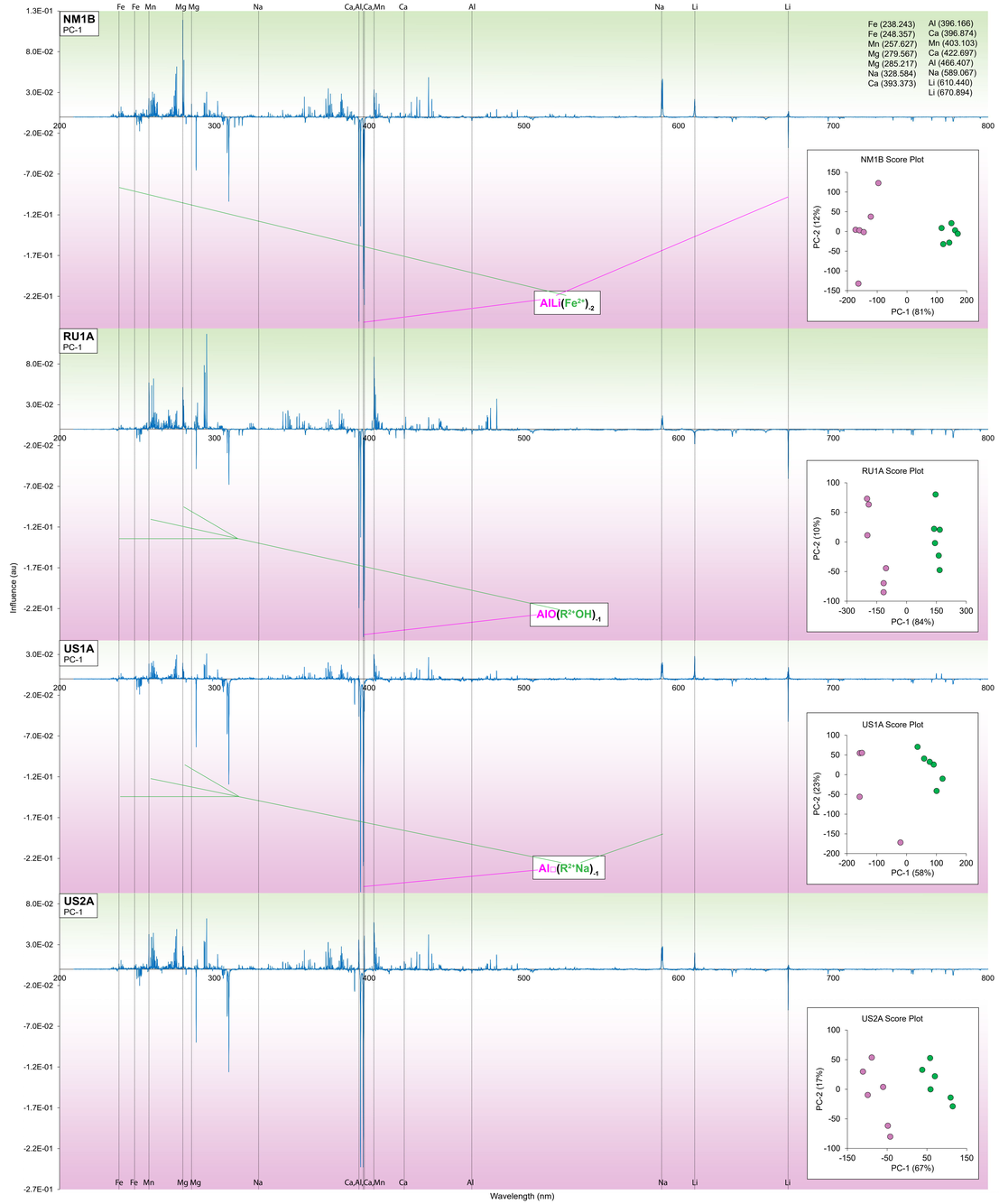

Figure 1. Principal component loading plots for samples NM1B, RU1A, US1A, and US2A as derived from PCA modeling of LIBS data. Each loading plot shows the influence of wavelength along principal component-1 (PC-1). The y-axis illustrates the relative proportion of influence, and the direction indicates whether a wavelength and a principal component are positively (enrichment in the green zone) or negatively (enrichment in the pink zone) correlated.

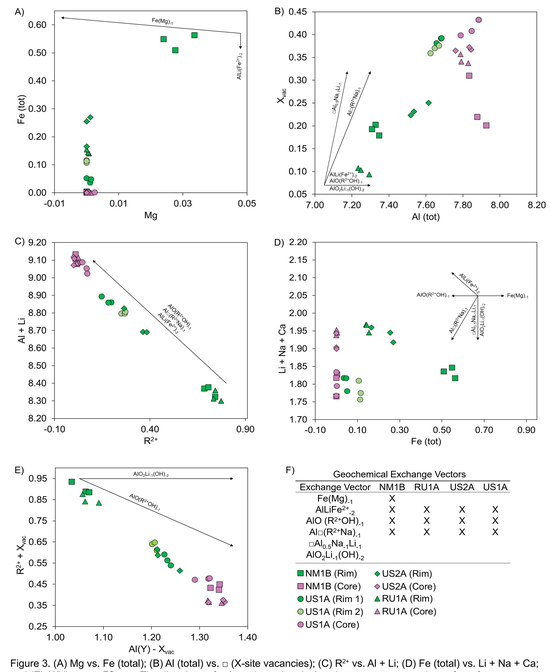

Figure 3. (A) Mg vs. Fe (total); (B) Al (total) vs. □ (X-site vacancies); (C) R^{2+} vs. Al + Li; (D) Fe (total) vs. Li + Na + Ca; and (E) Al(Y) - □ vs. R^{2+} + □. The directions of selected geochemical exchange vectors are shown for reference.

LIBS Results and Discussion

- Principal component analysis (PCA) of LIBS spectra was used to evaluate compositional differences between cores and rims without determination of actual elemental concentrations.
- Each score plot evaluates the compositional variations between the pink and green zones of individual samples: NM1B, RU1A, US1A, and US2A, evident in Figure 1, where the pink and green zones form distinct groups separated along the PC-1 axis of each sample.
- The loading plots for these samples (Fig. 1) depict the relative influence of each variable (i.e., wavelength) on the direction of PC-1 through the dataset of a sample.
- Loading plots can be data-mined to determine the relative elemental enrichment/depletion trends for the groupings (green rim zone vs. pink core zone) determined by PCA.
- Here wavelength markers are used to depict several of the influential elements, on the LIBS loading plots, that are involved in various geochemical exchanges between the core and rim zones of each sample as determined by vectors in the EMPA bivariate plots.

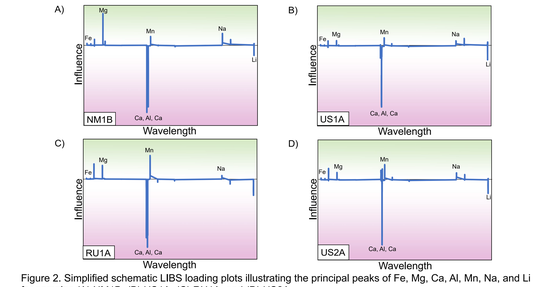

Figure 2. Simplified schematic LIBS loading plots illustrating the principal peaks of Fe, Mg, Ca, Al, Mn, Na, and Li for samples (A) NM1B, (B) US1A, (C) RU1A, and (D) US2A.

- Preliminary results indicate that LIBS PCA score and loading plots generally produce congruent results with exchange vectors plotted on EMPA bivariate diagrams. For example, PCA of LIBS spectra show that the core zones are consistently higher in: Al, Li, and Ca and lower in: Mn, Mg, Fe, and Na relative to rims (Fig. 3). This is consistent with the $AlLi(Fe^{2+})_{-2}$, $AlO(R^{2+}OH)_{-1}$, and $Al\square(R^{2+}Na)_{-1}$ geochemical exchange vectors depicted in the EMPA bivariate diagrams (Fig. 2) observed to describe core and rim compositions.
- Here it is important to note that Mn is commonly purported to be the principal chromophore in pink tourmaline zones; however, it appears here to be concentrated in the rim zones. Similar results were observed by Tollefson and Ihinger (2017, 2018 GSA Abstracts with Prog.) with the possible explanation that the oxidation state of Mn, rather than concentration, plays a large role in producing color.
- Further analysis is required to extract a more detailed record of compositional trends as they relate to changes in the environment of crystallization. Specifically, variations in element concentrations that are below the detection limit for EMPA but are recorded in the LIBS spectra and the role of oxygen fugacity as it relates to Mn and Fe.

EMPA Results and Discussion

- Substitutions that control chemical zoning in tourmaline during crystallization were evaluated by plotting bivariate composition diagrams of the EMPA data and establishing geochemical exchange vectors.
- Plot Mg vs. Fe (total) (Fig. 3a) generally shows a vertical trend, where the rim zone displays Fe enrichment, and the core zone experiences Fe depletion. Sample NM1B may have a combination of vectors $AlLi(Fe^{2+})_{-2}$ and $Mg(Fe)_{-1}$ acting on the sample however here it is important to note that Mg content is very close to the EMPA detection limit.
- Plot Al (total) vs. □ (Fig. 3b) displays a positive trend, where the core zone shows an increase in X-site vacancies alongside total Al content. This increase in X-site vacancies could be related to concurrent crystallization of Na-rich minerals which cause Na depletion within the system (Roda-Robles et al., 2015).
- Plot R^{2+} vs. Al + Li (Fig. 3c) displays a strong negative trend indicating that the core zone becomes enriched in Li and Al during crystallization, via a combination of the alkali defect substitution $Al\square(R^{2+}Na)_{-1}$ and the proton loss substitution $AlO(R^{2+}OH)_{-1}$ (Roda-Robles et al., 2015). This conclusion is further supported by plots Al (total) vs. □ (Fig. 3b) and Fe (total) vs. Li + Na + Ca (Fig. 3d).

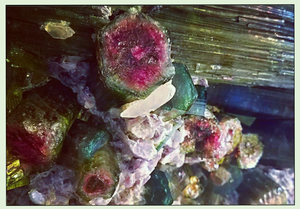

Future Work

- Analyze nine samples from a variety of localities to determine the consistency of compositional trends in tourmalines from pegmatites worldwide.
- Compare LIBS and EMP analyses of the samples to explore the relationship between EMPA and LIBS data.
- Investigate the role of Fe oxidation, and by inference, Mn oxidation states as they relate to the geochemical evolution of watermelon tourmaline using X-ray absorption near-edge structure (XANES) spectroscopy.

Acknowledgments

This research would not have been possible without the assistance of Dr. Barb Dutrow and Lab Manager Matthew Loocke at Louisiana State University in conjunction with the amazing staff at the Materialytics Lab in Killeen, Texas.

Conference related travel expenses were financed by the GSA Mineralogy, Geochemistry, Petrology, & Volcanology (MGPV) Division and New Mexico State University.

This research was supported (in part) by the Dora Blossom Gile Endowed Memorial Scholarship and the Greg Mack Endowed Scholarship at New Mexico State University.

References

CAMECA Science & Metrology Solutions, 2022, Introduction to EMPA: https://www.cameca.com/products/epma/technique (Accessed September 2022).

Gibson, M., and McMillan, N. J., 2019, A Compositional Analysis of Zoned Watermelon Tourmalines Using Laser-Induced Breakdown Spectroscopy (LIBS): Geological Society of America Abstracts with Programs, v. 51(5), doi: 10.1130/abs/2019AM-339497.

Gibson, M., and McMillan, N. J., 2020, A Compositional Analysis of Zoned Watermelon Tourmalines Using Laser-Induced Breakdown Spectroscopy (LIBS): Geological Society of America Abstracts with Programs, v. 52(6), doi: 10.1130/abs/2020AM-356403.

Henry, D. J., and Dutrow, B. L., 1996, Metamorphic tourmaline and its petrologic applications, in Grew, E. S., and Anovitz, L. M., eds., Boron: mineralogy, petrology and geochemistry, Volume 33: Washington, D.C., Mineralogical Society of America, p. 503-557.

McMillan, N. J., Montoya, C., and Chesner, W. H., 2012, Correlation of limestone beds using laser-induced breakdown spectroscopy and chemometric analysis: Applied Optics, v. 51, p. B213-B222.

Roda-Robles, E., Simmons, W., Pesquera, A., Gil-Crespo, P., Nizamoff, J., and Torrez-Ruiz, J., 2015, Tourmaline as a petrogenetic monitor of the origin and evolution of the Berry-Havey pegmatite (Maine, U.S.A.): American Mineralogist, v. 100, p. 95-109.

Tollefson, K.T., and Ihinger, P.D., 2017, The Cause of Color Variation in Watermelon Tourmaline: Insights from Infrared Spectroscopy: Geological Society of America Abstracts with Programs, v. 49, no. 6, ISSN 0016-7592 doi: 10.1130/abs/2017AM-308641.

Tollefson, K.T., and Ihinger, P.D., 2018, Evolving Growth Conditions for Watermelon Tourmaline: Elemental Abundance Patterns Tell the Story: Geological Society of America Abstracts with Programs, v. 50, no. 6, ISSN 006-7592 doi: 10.1130/abs/2018AM-321255.